Interfacial Engineering of Graphene Oxide Immobilization on Polylactic Acid Substrates through Surface Modification

Student: Jiwei (Aaron) Bai
St. George's School, Vancouver, BC, Canada

Instructor: Jie Song
College of Innovation and Technology, University of Michigan-Flint
Flint, MI, USA

August 22, 2026

Declaration of Academic Integrity

The participating team declares that the paper submitted is comprised of original research and results obtained under the guidance of the instructor. To the team's best knowledge, the paper does not contain research results, published or not, from a person who is not a team member, except for the content listed in the references and the acknowledgment. If there is any misinformation, we are willing to take all the related responsibilities.

Names of team members: Jiwei (Aaron) Bai

Signatures of team members: 

Name of the instructor: Jie Song

Signature of the instructor: 

Date: 08/18/2026.

INTERFACIAL ENGINEERING OF GRAPHENE OXIDE IMMOBILIZATION ON POLYLACTIC ACID SUBSTRATES THROUGH SURFACE MODIFICATION

J. W. Bai

St. George's School, Vancouver V6S1V1, Canada

Graphene oxide (GO) exhibits strong adsorption capability for dye removal, but its practical utilization remains constrained by aggregation and poor recoverability in aqueous systems. In this study, GO was immobilized onto biodegradable polylactic acid (PLA) through an interfacial engineering strategy. PLA substrates were first activated by alkaline etching to increase surface roughness and energy, followed by 3-aminopropyltriethoxysilane (KH550) silanization to enhance interfacial adhesion. GO was then deposited onto the modified PLA via ultrasonic-assisted coating. The as-prepared composite was systematically characterized using SEM, FTIR, Raman spectroscopy, and XRD, confirming successful GO immobilization. Stability tests demonstrated that the composite retained 93.7% and 81.5% of its initial GO loading in aqueous and acidic environments after 13 days, respectively. Methylene blue (MB) adsorption experiments revealed kinetics following the pseudo-second-order model with adsorption equilibrium reached within approximately 60 min. The adsorption data were well described by the Langmuir isotherm model, yielding a maximum adsorption capacity of 197.21 mg·g^{-1}, indicative of monolayer adsorption. After six adsorption–desorption cycles, the composite retained 75.2% of its initial adsorption capacity, indicating satisfactory reusability. This work developed a surface-engineered GO–PLA composite through an effective surface modification strategy, generating a stable and reusable material whose functional performance was validated by the adsorption experiments.

***Keywords*:** polylactic acid (PLA), graphene oxide (GO), interfacial engineering, silane coupling agent, methylene blue (MB), surface modification.

Table of Contents

1. Introduction 3
2. Materials and Methods 4
    2.1. Materials 4
    2.2. NaOH Etching Optimization Based on Orthogonal Experiment 4
    2.3. Preparation of the GO–PLA Composite 5
    2.4. Characterization 5
    2.5. Water Resistance and Acid Resistance Tests 6
    2.6. Adsorption of Methylene Blue (MB) 6
    2.7. Cyclic Adsorption–Desorption Performance of GO–PLA Composite 7
3. Results and Discussion 7
    3.1. Effect of NaOH Etching on Surface Morphology and Surface Energy of PLA 7
    3.2. Interfacial Immobilization and Structural Characterization of GO–PLA 9
    3.3. GO Loading and Environmental Stability of the Composite Coating 10
    3.4. Adsorption Behavior of GO–PLA Towards MB 11
    3.5. Reusability of the GO–PLA Composite 13
    3.6. Performance Comparison of GO-based Composite Adsorbents 13
    3.7. Proposed Adsorption Mechanism 14
4. Conclusion 16
5. References 16

1. Introduction

The rapid development of industrial activity and urban expansion has led to a significant increase in dye-containing wastewater discharge. Synthetic organic dyes are regarded as particularly problematic contaminants because of their high chromaticity, complex chemical structures, and resistance to natural degradation [1]. Adsorption has been widely regarded as an effective and practical method for dye removal due to its operational simplicity and high treatment efficiency [2]. However, adsorption performance is strongly dependent on the structural stability, surface properties, and reusability of the adsorbents [3]. Therefore, the development of stable and functional adsorbent materials through surface engineering and material modification has attracted considerable research attention in recent years.

Graphene oxide (GO), a derivative of graphene enriched with abundant oxygen-containing functional groups, such as hydroxyl, epoxy, and carboxyl groups, has emerged as a promising candidate for adsorptive removal of organic pollutants [4]. The large specific surface area, excellent chemical stability, and strong interaction capability of GO with various organic molecules make it particularly suitable for capturing dye molecules through multiple interactions, such as π–π stacking, hydrogen bonding, and electrostatic attraction [5]. Previous studies have demonstrated the high adsorption capacities of GO toward different types of dyes, especially cationic dyes such as methylene blue (MB) [6, 7]. However, despite its excellent adsorption performance, the practical application of GO in water treatment systems remains constrained by several inherent limitations [8]. First, GO is typically available in powder or nanosheet form, which makes it difficult to separate from aqueous solutions after dispersion [9]. Second, GO sheets are prone to aggregation driven by strong van der Waals forces and π–π interactions between layers, resulting in a reduced effective surface area and decreased adsorption efficiency [10, 11]. Third, the direct use of GO as a suspended adsorbent may cause secondary pollution, further complicating water treatment processes [12]. Consequently, developing a reliable method to immobilize GO onto a stable and environmentally friendly support substrate is highly desirable for enhancing its practical applicability [13, 14].

Recently, biodegradable polymer materials have attracted growing attention due to their environmental sustainability and versatile applications. Among them, polylactic acid (PLA) is one of the most widely used bio-based polymers owing to its biodegradability, non-toxicity, and environmental friendliness [15]. PLA is derived from renewable resources such as corn starch or sugarcane and has been widely utilized in packaging, biomedical devices, and environmental applications, providing a promising platform for constructing sustainable materials with potential applications in environmental remediation [16]. However, pristine PLA generally exhibits a smooth surface, low surface energy, and limited chemical reactivity, which significantly restricts its ability to directly bind or immobilize functional nanomaterials such as GO [17]. As a result, effective surface modification or interfacial engineering are necessary to enhance its surface activity and improve its compatibility with functional coatings [18, 19]. Previous studies have reported GO-modified PLA systems for adsorption applications [6, 13, 17]. However, most of them rely on physical deposition or weak interactions, which often suffer from GO detachment and limited cycling stability. In contrast, the present work introduces a surface activation–coupling strategy to achieve stable chemical anchoring of GO on PLA, significantly improving interfacial robustness and

reusability.

Surface engineering has been proven to be a promising approach for modifying the physicochemical properties of polymer materials without altering their bulk structure [20]. In particular, alkaline etching using sodium hydroxide (NaOH) can introduce microscale surface roughness and expose polar functional groups on polymer surfaces, thereby increasing surface energy and enhancing wettability [21, 22]. Furthermore, the introduction of silane coupling agents, such as 3-aminopropyltriethoxysilane (KH550), can serve as chemical bridges between inorganic nanomaterials and organic substrates via the formation of covalent bonds, resulting in improved interfacial adhesion and coating stability [23].

By integrating physical etching and chemical coupling strategies, it becomes possible to rationally tailor the interfacial properties of PLA in order to construct a stable and uniform GO coating. Such a design concept combines the structural advantages of a PLA scaffold with the functional performance of GO, thereby creating a composite material with synergistically enhanced adsorption capabilities [24]. However, for PLA-supported GO systems, the relationship between surface activation, interfacial coupling, GO loading, and coating stability has not yet been sufficiently clarified. The practical applicability of such materials in aqueous environments remains limited by possible coating loss and insufficient understanding of the substrate–coating interaction.

In this work, a sustainable GO–PLA composite was constructed through a rational interfacial strategy. First, the surface energy and roughness of the PLA substrate were regulated by NaOH etching, followed by surface functionalization using KH550 to enhance interfacial bonding. Subsequently, GO was immobilized onto the modified PLA surface via ultrasonic-assisted dip-coating to form a stable and uniform functional layer. The effective formation of the GO–PLA composite was confirmed by SEM, FTIR, Raman spectroscopy, and XRD analyses. More importantly, the study focused not only on the fabrication of the composite itself, but also on clarifying how interfacial modification affects GO immobilization, environmental stability, and adsorption behavior.

2. Materials and Methods

2.1. Materials. All reagents used in this study were of analytical grade and were applied directly without any additional purification. Polylactic acid (PLA) plates served as the substrate. Sodium hydroxide (NaOH), hydrochloric acid (36 wt.%), graphene oxide (GO, powder), methylene blue (MB), absolute ethanol, diiodomethane, and KH550 were purchased from Shanghai Titan Technology Co., Ltd. Deionized water was used as the universal solvent throughout all experimental procedures. All measurements were performed at room temperature, and each test was repeated at least three times to ensure the reliability of the results. The experiment was repeated for 3 times, and the data were presented as mean ± SD (n = 3).

2.2. NaOH Etching Optimization Based on Orthogonal Experiment. Before surface etching, PLA plates (3 × 3 cm) were first subjected to ultrasonic-assisted cleaning in absolute ethanol (35 kHz, 200 W) for 10 min, rinsed three times with deionized water, and dried at 60 °C for 6 h. To optimize the alkaline etching process, an $L_9(3^4)$ orthogonal experimental design was applied to three factors: NaOH concentration (2, 4, and 6 wt.%), etching temperature (50, 60, and 70 °C), and etching time (20, 40, and 60 min). Surface wettability was assessed by contact angles with water and diiodomethane, and surface free energy (γ_s) and its dispersive/polar components

was calculated via the Owens–Wendt model on ≥5 measurements per sample, with factor significance determined by K and R values in orthogonal analysis [25].

$$\frac{(1+\cos\theta)\gamma_l}{2} = (\gamma_s^d + \gamma_l^d)^{\frac{1}{2}} + (\gamma_s^p + \gamma_l^p)^{\frac{1}{2}} \ ; \quad (1)$$

$$\gamma_s = \gamma_s^d + \gamma_s^p \ ; \quad (2)$$

where γ_s and γ_l represent the surface free energies of the solid and liquid, respectively. γ_s^d and γ_s^p denote the dispersive and the polar components of the solid surface energy, while γ_l^d and γ_l^p correspond to those of the liquid. θ is the contact angle.

2.3. Preparation of the GO–PLA Composite. The fabrication process is illustrated in Fig. 1. NaOH-etched PLA plates were immersed in a KH550 ethanol solution (1 wt.%) and treated at 25 °C for 30 min. Subsequently, the plates were rinsed three times with absolute ethanol to remove unbound KH550, dried at 60 °C for 30 min, and then heated at 80 °C for 1 h to promote curing, forming covalent Si–O–C bonds. A GO dispersion (2 wt.%) was prepared by dispersing GO in deionized water containing 0.1 wt.% KH550 (relative to GO). The modified PLA substrates were then immersed in the GO suspension and subjected to ultrasonic irradiation (35 kHz, 200 W) for 2 h to facilitate uniform deposition. After treatment, the PLA plates were cured at 80 °C for 2 h, yielding the GO–PLA composite.

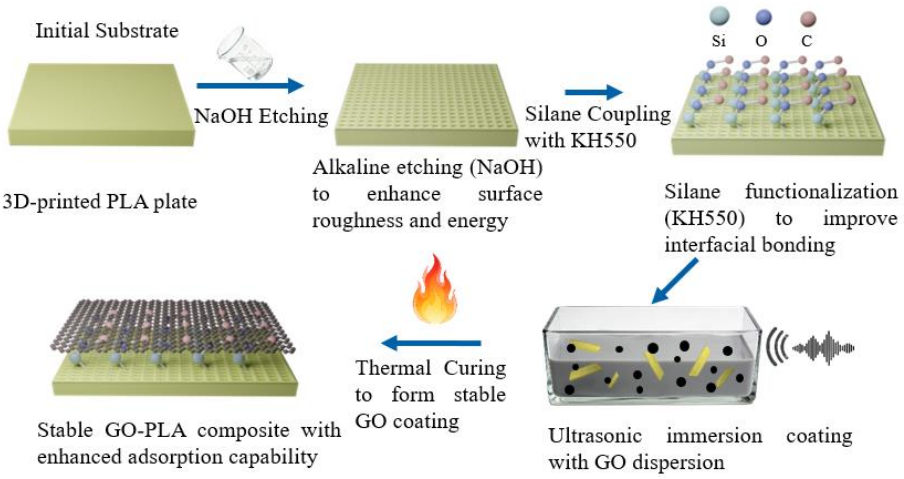


Fig. 1. Schematic diagram of NaOH etching and GO immobilization on the PLA substrate.

2.4. Characterization. The surface morphology of both PLA and GO–PLA samples was examined using scanning electron microscopy (SEM) (5kV accelerating voltage, gold-sputtered samples). Fourier transform infrared spectroscopy (FTIR) in ATR mode (4000–500 cm^{-1}, 4 cm^{-1} resolution, 32 scans) was used to identify characteristic functional groups and verify the surface modification of PLA as well as the successful immobilization of GO. Raman spectroscopy (532 nm, 500–3500 cm^{-1}, disorder evaluated by I_D/I_G) was used to further confirm the structural characteristics of GO and to analyze the degree of disorder of the carbon-based materials. X-ray diffraction (XRD) (Cu Kα, λ=0.15418 nm, 5°–55°, 0.02° step) measurements were conducted to investigate the crystalline structure and structural changes of the samples before and after modification

2.5. Water Resistance and Acid Resistance Tests. The GO–PLA composite was separately immersed in two different media, including 500 mL of deionized water and 500 mL of hydrochloric acid solution (0.05 mol·L^{-1}) at 25 °C in the dark. The exposure time varied from Day 1 to Day 13 to evaluate stability over time. Samples were retrieved every two days, rinsed, dried, weighed, and the areal loading calculated.

$$\Gamma = (m_f - m_i)/A, \tag{3}$$

where Γ (g·m^{-2}) represents the GO loading per unit area on the PLA substrate, $m_i$is the initial mass of the GO–PLA composite, and m_f is the residual mass after immersion in water or acid solution for a given period (n days). A is the surface area of the PLA substrate.

2.6. Adsorption of Methylene Blue (MB). Adsorption experiments were conducted using 50 mL MB solutions at 25 ± 0.5 °C. GO–PLA composites containing 20 mg of immobilized GO were used as the adsorbent. Periodically, supernatant aliquots (3 mL) were taken and passed through 0.22 μm filters. MB concentration was measured by UV-vis spectroscopy at 664 nm using a pre-calibrated standard curve.

The adsorption removal rate R (%) and adsorption capacity Q_e (mg·g^{-1}) were calculated using the following formulas:

$$Q_e = \frac{(C_0\text{-}C_e)\times V}{m}, \tag{4}$$

where C_0 is the initial concentration of MB (mg·L^{-1}), C_e is the equilibrium concentration of MB (mg·L^{-1}), V is the volume of MB solution (L), and m is the mass of the adsorbent (g).

To investigate the adsorption kinetics, both pseudo-first-order and pseudo-second-order models were adopted to describe the adsorption behavior. Kinetic experiments were carried out using an MB solution with an initial concentration of 30 mg·$L^{-1,}$ and the adsorption process was monitored from 0-100 min.

$$Q_t = Q_e(1 - e^{-k_1 t}), \tag{5}$$

$$Q_t = \frac{k_2 Q_e^2 t}{1 + k_2 Q_e t}, \tag{6}$$

where Q_e (mg·g^{-1}) is the equilibrium adsorption capacity, Q_t (mg·g^{-1}) is the adsorption capacity at time t (min), k_1 (min^{-1}) is the pseudo-first-order adsorption rate constant, and k_2 (g·mg^{-1}·min^{-1}) corresponds to the pseudo-second-order adsorption rate constant.

Langmuir and Freundlich models were employed to interpret the adsorption isotherms. Isotherms experiments were carried out using an MB solution with an initial concentration from 10 to 90 mg·L^{-1}. Samples were collected and analyzed after equilibrium.

$$Q_e = \frac{K_L Q_{max} C_e}{1 + K_L C_e} \tag{7}$$

$$Q_e = K_F C_e^{\frac{1}{n}} \tag{8}$$

where Q_e ($mg \cdot g^{-1}$) is the equilibrium adsorption capacity, C_e ($mg \cdot L^{-1}$) is the equilibrium concentration of adsorbate in solution, Q_{max} ($mg \cdot g^{-1}$) is the maximum monolayer adsorption capacity, and K_L ($L \cdot mg^{-1}$) is the Langmuir adsorption constant; K_F is the Freundlich constant, and $1/n$ is the heterogeneity factor indicating adsorption intensity.

2.7. Cyclic Adsorption–Desorption Performance of GO–PLA Composite. The recyclability of the GO–PLA composite was evaluated through repeated adsorption–desorption cycles in MB solution (50 mL, 25 ± 0.5 °C) with an initial concentration of 30 $mg \cdot L^{-1}$. Each adsorption step was conducted for 24 h to ensure equilibrium uptake. After equilibrium, the loaded adsorbent was physically separated from the solution and regenerated by immersion in 50 mL of absolute ethanol for 2 h to remove the adsorbed dye species. After desorption, the adsorption step was repeated 6 cycles, and the retention of adsorption capacity after each cycle was calculated.

$$\eta = \frac{Q_n}{Q_1} \times 100\% \quad (9)$$

where Q_n ($mg \cdot g^{-1}$) is the adsorption capacity in cycle *n*, and Q_1 ($mg \cdot g^{-1}$) is the adsorption capacity in the first cycle.

3. Results and Discussion

3.1. Effect of NaOH Etching on Surface Morphology and Surface Energy of PLA. Table 1 summarizes the orthogonal test results for NaOH etching. The range analysis ranked the three factors as follows: NaOH concentration (R = 41.20) > temperature (R = 29.79) > time (R = 11.29). NaOH concentration is the dominant factor in regulating the surface energy of PLA, while temperature and time show secondary effects. Among all the tested conditions, sample 3 (6 wt.% NaOH, 70 °C, 20 min) and sample 4 (6 wt.% NaOH, 60 °C, 40 min) exhibited significantly higher surface energy values of 73.42 $mN \cdot m^{-1}$ and 73.35 $mN \cdot m^{-1}$, respectively. In contrast, the mildly treated samples (e.g. sample 1 and sample 5) showed much lower surface energy values, indicating limited surface activation under weak etching conditions.

TABLE 1. Results of the orthogonal test for NaOH etching

No.	Factor A	Factor B	Factor C	Surface energy ($mN \cdot m^{-1}$)	Water contact angle (θ)	Diiodomethane contact angle (θ)	Dispersive components (mJ/m^2)	Polar components (mJ/m^2)
	NaOH (wt.%)	Temp (°C)	Time (min)					
1	2	50	20	8.35	108.3	123.8	2.50	5.85
2	4	60	20	14.04	92.2	115.1	4.20	9.84
3	6	70	20	73.42	74.9	0	72.64	0.71
4	6	60	40	73.35	72.7	0	72.33	1.09
5	4	50	40	10.87	106.8	103.4	7.51	3.36
6	2	70	40	29.45	87.7	65.5	25.44	4.01
7	2	60	60	14.94	91.2	114.0	4.47	10.47

8	4	70	60	35.36	79.0	59.4	28.78	6.58
9	6	50	60	29.57	86.3	66.4	24.89	4.68
K1	17.58	16.26	31.93					
K2	20.09	34.13	37.91					
K3	58.78	46.05	26.62					
R	41.2	29.79	11.29					

Figure 2 shows the SEM images of PLA surfaces treated under different NaOH etching conditions. Under mild etching conditions, only limited surface changes were observed. For sample 1 (2 wt.% NaOH, 50 °C, 20 min) exhibited only a few shallow pits, and the surface remained relatively smooth and compact. With increasing NaOH concentration and temperature, the etching effect became more pronounced, leading to the formation of irregular pits and a rougher surface morphology.

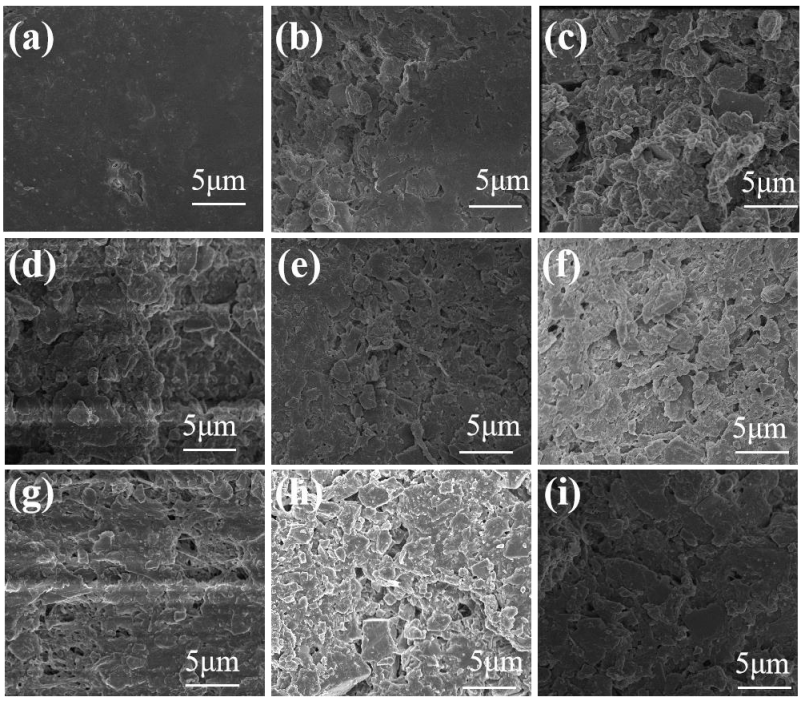


Fig. 2. SEM images of PLA samples after NaOH etching under different conditions: (a) 2 wt.% NaOH, 50 °C, 20 min; (b) 4 wt.% NaOH, 60 °C, 20 min; (c) 6 wt.% NaOH, 70 °C, 20 min; (d) 6 wt.% NaOH, 60 °C, 40 min; (e) 4 wt.% NaOH, 50 °C, 40 min; (f) 2 wt.% NaOH, 70 °C, 40 min; (g) 2 wt.% NaOH, 60 °C, 60 min; (h) 4 wt.% NaOH, 70 °C, 60 min; and (i) 6 wt.% NaOH, 50 °C, 60 min.

A further increase in etching severity caused clear surface damage. In sample 3 (6 wt.% NaOH, 70 °C, 20 min), the PLA surface showed extensive pit formation together with partial powdering, indicating over-etching and structural degradation. Although this condition produced the highest surface energy, the PLA's structural integrity was significantly compromised, which is unfavorable for the stable immobilization of a GO coating. By contrast, sample 4 (6 wt.% NaOH, 60 °C, 40 min) and sample 8 (4 wt.% NaOH, 70 °C, 60 min) exhibited abundant

and uniformly distributed micro-scale pits without noticeable cracking or powdering of the PLA substrate. These microstructures enlarge the effective surface area and provide anchoring sites for GO attachment. Compared with sample 8, sample 4 exhibited a higher surface energy (73.35 $mN \cdot m^{-1}$) while maintaining good structural integrity. These surface attributes not only expand the accessible area but also offer abundant potential binding loci for GO anchoring [26].

Taking into account both surface energy and morphological characteristics, we chose sample 4 (6 wt.% NaOH, 60°C, 40 min) as the optimal etching regime for subsequent functionalization and GO deposition. Under these conditions, the etched PLA substrate possesses a high surface energy and a favorable microstructure, which provides an ideal foundation for the formation of a stable and uniformly distributed GO coating.

3.2. Interfacial Immobilization and Structural Characterization of GO–PLA. The GO coating on the modified PLA surface was observed using a scanning electron microscope (SEM), as shown in Fig. 3. GO exhibited a flaky stacking morphology and was uniformly distributed on the modified PLA plates. Only minor localized detachment was observed, indicating that the deposited GO formed a relatively continuous coating layer on the substrate. Combined with the etched microstructure generated during NaOH treatment, the modified PLA surface provided sufficient anchoring sites, thereby facilitating stable immobilization of GO.

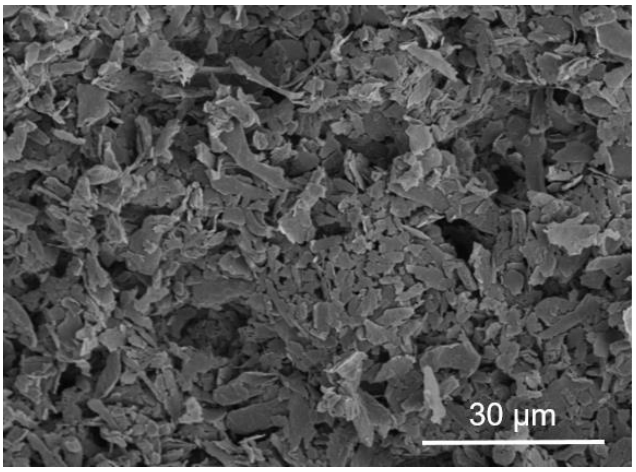


Fig. 3. SEM of GO-PLA Samples.

The chemical structure changes during surface modification were analyzed by FTIR spectroscopy in Fig 4a. Pristine PLA exhibited a characteristic absorption peak at 1750 cm-1 corresponding to the stretching vibration of C=O groups. The bands at 1450 cm^{-1} and 1380 cm-1 are attributed to the bending vibrations of $–CH_3$ groups, while the peaks at 1260 cm-1 and 1180 cm-1 are assigned to C–O–C bonds [27]. After NaOH treatment, a new absorption peak appears at 1500–1600 cm^{-1}, which can be ascribed to carboxylate groups ($–COO^–$) generated by the hydrolysis of PLA ester bonds [28]. In addition, the –OH stretching band near 3500 cm^{-1} is significantly enhanced, while the intensity of C=O at 1750 cm^{-1} decreases. NaOH treatment induces the hydrolysis of ester bonds in PLA, resulting in an increase in surface hydroxyl groups.

After KH550 modification, the absorption feature in the 1500–1600 cm^{-1} and the –OH band at 3500 cm^{-1} decrease. Meanwhile, new absorption signals in the 1000–1100 cm^{-1} can be attributed to vibrations of Si–O–C

bonds and Si–O–Si bonds [29], confirming successful grafting of silane coupling groups onto the PLA surface. For the PLA+NaOH+KH550+GO composite, the overall FTIR intensity decreases, which is mainly attributed to the shielding effect of the deposited GO layers on the modified substrate. No obvious new characteristic peaks or significant peak shifts are observed, likely due to functional group overlap and the relatively low GO content.

Further evidence for GO loading was obtained from Raman spectroscopy in Fig. 4b. Pure PLA, PLA+NaOH, and PLA+NaOH+KH550 show C–H stretching vibration peaks near 2900 cm^{-1}, and no graphitic carbon-related characteristic peaks are observed. In contrast, the PLA+NaOH+KH550+GO composite shows two distinct peaks of GO at approximately 1350 cm^{-1} (D band) and 1580 cm^{-1} (G bands) of GO. The D band is associated with structural defects of sp^3-hybridized carbon atoms in GO structure, while the G band originates from the in-plane vibration of sp^2-hybridized carbon atoms in the GO framework.

Figure 4c shows the XRD patterns of the samples. The pure PLA sample exhibits distinct diffraction peaks at 2θ = 16.5° and 2θ = 18.8°, which are attributed to the (110) and (200) crystal planes of the α-crystal form of PLA. After NaOH treatment and KH550 modification, the main diffraction patterns of PLA remain largely unchanged, indicating that the chemical treatments mainly affect the surface of the material without significantly altering its bulk crystalline structure. In the PLA–NaOH–KH550–GO composite, the typical diffraction features of PLA are retained, while a distinct peak at 2θ = 10.8°, corresponding to the (001) plane of GO, is observed. In contrast, pure GO exhibits a sharper and more intense diffraction peak, reflecting its well-defined layered structure. In the composite, the GO peak slightly shifted to the left and became weakened and broadened, indicating that GO sheets are highly dispersed on the PLA surface rather than existing in a stacked crystalline form. Such dispersion is beneficial for maximizing the exposure of active adsorption sites.

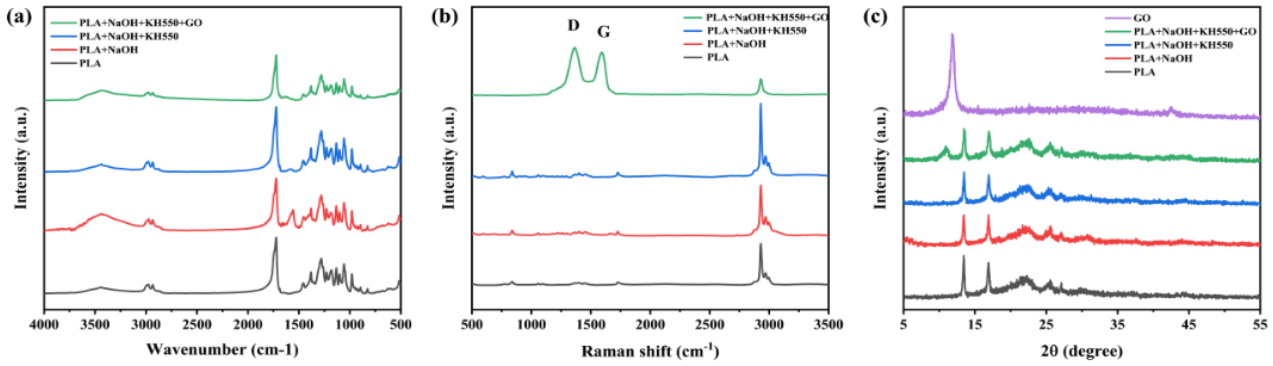


Fig. 4. (a) FT-IR spectra (b) Raman spectroscopy, (c) XRD patterns of PLA, PLA+NaOH, PLA+NaOH+KH550, and PLA+NaOH+KH550+GO.

3.3. GO Loading and Environmental Stability of the Composite Coating. The loading stability of GO on different PLA-based substrates was systematically evaluated to clarify the effectiveness of surface modification on GO immobilization. As shown in Fig. 5a, pure PLA exhibited the lowest GO loading, at 2.6 $g \cdot m^{-2}$, indicating its relatively smooth surface and hydrophobic nature are unfavorable for GO immobilization. After NaOH etching, the GO loading increased to 5.0 $g \cdot m^{-2}$, which can be attributed to the formation of polar surface groups and a rougher microstructure that provided more active sites for GO anchoring [14]. The PLA+NaOH+KH550 sample

shows the highest GO loading at 9.3 g·m⁻². The introduction of the silane coupling agent further enhances the interfacial interaction between GO and the PLA substrate through chemical bonding and hydrogen-bonding interactions. These results confirm the crucial role of the combined alkaline etching and silane modification in improving the GO immobilization capacity of PLA [30].

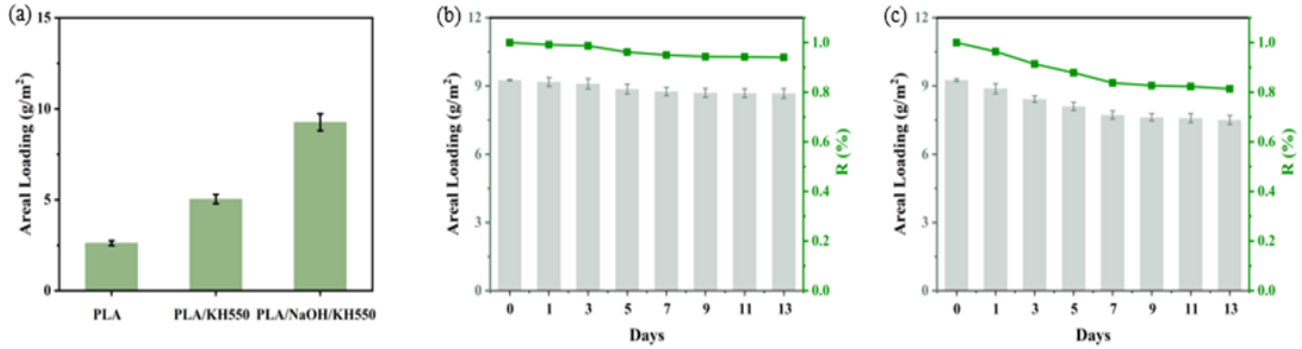


Fig. 5. Comparison of GO areal mass loadings on PLA, PLA+NaOH, and PLA+NaOH+KH550 (a), stability of the GO layer immersed in water (b) and under acidic conditions (c). All data are presented as mean ± SD (n = 3).

The environmental stability of the GO layer was further evaluated by monitoring the remaining GO loading during immersion. As shown in Fig 5b, under pure water conditions, the GO loading on the PLA+NaOH+KH550 sample gradually decreased from 9.3 to 8.7 g·m^{-2}, corresponding to 93.7% retention of the initial loading. The interfacial interactions between GO and the modified PLA substrate are strong enough to resist significant detachment in water, which is crucial for the application stability in water systems. In an acidic environment, the GO loading on the composite exhibits a more rapid and continuous decline from 9.2 to 7.5 g·m^{-2}, as illustrated in Fig 5c. This accelerated loss of GO in acidic solution is mainly attributed to partial protonation of oxygen-containing functional groups on GO, weakened interfacial adhesion, and potential hydrolytic instability of the silane coupling agents under acidic attack. Despite the harsher acidic conditions, 81.5% of the initial GO loading was retained after 13 days, indicating strong interfacial adhesion induced by the surface engineering treatment. The combined NaOH etching and KH550 modification strategy not only enhances the initial GO loading but also significantly improves the long-term stability of the coating [31].

3.4 Adsorption Behavior of GO–PLA Towards MB. The adsorption behavior of the GO–PLA composite toward MB was evaluated using kinetic and isotherm models. As illustrated in Fig 6a, the adsorption capacity increased rapidly at the initial stage and gradually approached equilibrium at around 60 min. At the early stage of adsorption, abundant active sites are available on the composite surface, which enables rapid uptake of dye molecules. As the process proceeds, these active sites become progressively occupied, leading to a reduction in adsorption rate until equilibrium is reached [32, 33].

To further analyze the adsorption kinetics, the experimental data were fitted using pseudo-first-order and pseudo-second-order models (Table 2). The pseudo-second-order model gave a better fit than the pseudo-first-order model, with a higher R^2 value (0.98 vs. 0.92). In addition, the calculated equilibrium adsorption capacity from the pseudo-second-order model (52.10 mg/g) was slightly higher than that of the pseudo-first-order model

(48.56 mg/g). The adsorption process was better described by the pseudo-second-order model. The enhanced adsorption performance of GO–PLA is attributed to the presence of oxygen-containing functional groups on GO as well as interfacial interaction effects [17].

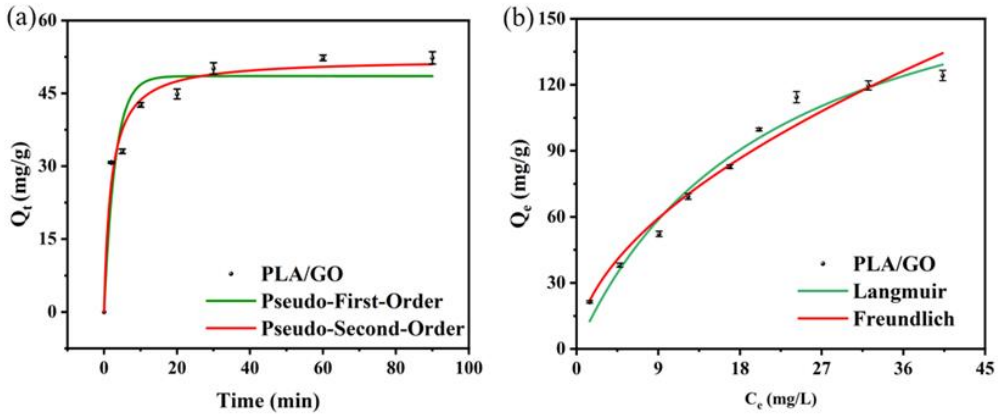


Fig. 6. (a) MB adsorption kinetics on GO–PLA with contact time of 0-100 min and non-linear fitting curves by pseudo-first-order model and pseudo-second-order model. (b) Adsorption isotherm of MB on GO–PLA composite fitted using Langmuir and Freundlich models. Data are presented as mean ± SD (n = 3).

TABLE 2. Kinetics model parameters of MB adsorption on GO–PLA

Pseudo-first-order kinetic			Pseudo-second-order kinetic		
Q_e (mg·g^{-1})	K_1 (min^{-1})	R^2	Q_e (mg·g^{-1})	K_2 (g·mg^{-1}·min^{-1})	R^2
48.56	0.33	0.92	52.10	0.0099	0.98

The adsorption isotherm behavior of MB on the GO–PLA composite is presented in Fig. 6b, and the experimental data were fitted using both Langmuir and Freundlich models. As summarized in Table 3, the Langmuir model exhibits slightly improved fitting performance, with a higher correlation coefficient (R^2 = 0.97) than the Freundlich model (R2 = 0.96). The adsorption of MB on the GO–PLA composite is better described by a monolayer adsorption process. The calculated Q_{max} of 197.21 mg·g^{-1} is comparable to other GO-based composites, namely magnetic cellulose-GO (70 mg·g^{-1} [34]), chitosan-GO (110.9 mg·g^{-1} [35]), and sulfanyl acid–magnetic GO (317 mg·g^{-1} [36]). The immobilization of GO on the PLA substrate effectively preserves its adsorption functionality.

By immobilizing GO onto a solid PLA substrate, the GO–PLA system also benefits from improved structural stability, easier recovery, and better material sustainability. The homogeneous distribution of GO across the functionalized PLA surface provides accessible adsorption sites, while the stable interfacial bonding helps maintain its effectiveness during adsorption.

TABLE 3. Langmuir and Freundlich isotherm parameters of MB adsorption onto GO–PLA

Langmuir			Freundlich		
Q_{max}(mg·g^{-1})	K_L(L·mg^{-1})	R^2	K_F	1/n	R^2
197.21	0.047	0.97	17.91	0.55	0.96

3.5. Reusability of the GO–PLA Composite. The GO–PLA composite was evaluated for reusability through six successive adsorption–desorption cycles for MB removal, as shown in Fig. 7. A gradual decline in adsorption efficiency was observed with increasing cycle number, with the highest value recorded in the first cycle. The decrease is more pronounced during the initial cycles, while the adsorption performance tends to stabilize after the third cycle. Even after six cycles, the composite retained 75.2% of its original adsorption capacity.

The gradual loss of performance can be mainly attributed to incomplete regeneration of active sites, partial shielding effects, or degradation of oxygen-containing functional groups on the GO surface during cyclic adsorption–desorption processes [37]. These changes lead to a reduction in the number of effective adsorption sites available for MB molecules. Nevertheless, the retained adsorption capacity remains comparable with that reported for similar GO-based composite adsorbents after repeated cycling [38]. Immobilization of GO on the PLA substrate helps maintain both the structural integrity and adsorption functionality of GO. Therefore, the GO–PLA composite exhibits satisfactory reusability and remains promising for repeated adsorption applications.

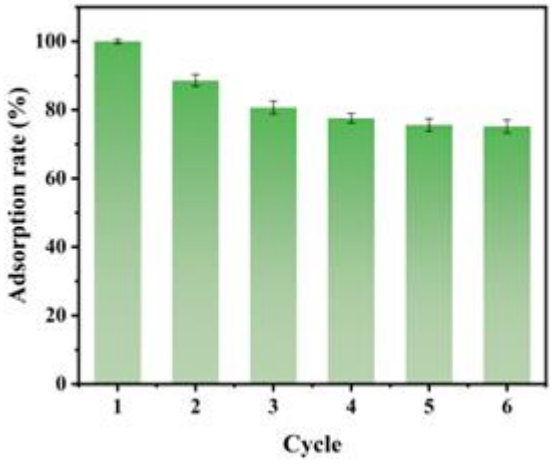


Fig. 7. Recycle test data for MB removal by GO–PLA. Data are presented as mean ± SD (n = 3).

3.6. Performance Comparison of GO-based Composite Adsorbents. To further evaluate the adsorption performance of the GO–PLA composite, recently reported GO-based adsorbents for MB removal are compared. As summarized in Table 4, the GO–PLA composite exhibits a competitive adsorption capacity (197.21 mg·g^{-1}) that exceeds most PLA-based GO adsorbents [34, 35, 39-42] and many other GO-based composites. Although some materials exhibit higher capacities (e.g., sulfanyl acid–magnetic GO at 317.3 mg·g^{-1} [36] and casein-GO at 437.3 mg·g^{-1} [43]), they often involve more complex preparation procedures or rely on forms that are less convenient for recovery.

The rigid PLA support in our system not only enables easy separation from treated water but also minimizes secondary pollution risks, highlighting the practical advantage of substrate-immobilized GO adsorbents. In summary, the GO–PLA system offers distinct practical advantages: (i) the macroscopic PLA substrate enables direct removal without centrifugation, filtration, or magnetic separation; (ii) the GO coating remains stable under both neutral and acidic conditions (93.7% and 81.5% retention) after 13 days; (iii) the PLA substrate is biodegradable, aligning with sustainable wastewater treatment principles.

TABLE 4. Performance comparison of GO-based composite adsorbents

Adsorbent	Q_{max} (mg·g-1)	Reusability	Adsorption time (min)	Recovery method	Reference
Magnetic cellulose–GO	70.0	5 cycles / ~89%	~ 180	Magnetic separation	[34]
Chitosan–GO	110.9	Not reported	~ 180	Direct removal	[35]
Fe_3O_4@GO@SA	317.3	Not reported	~ 240	Magnetic separation	[36]
Green-prepared rGO	121.95	Not reported	~ 30	Centrifugation/ Filtration	[39]
AIg-GO	120.37	8 cycles / ~96%	~ 30	Filtration	[40]
CMC-Alg/GO	78.5	4 cycles / ~76%	~ 90	Filtration	[41]
GO-zeolite	123.0	5 cycles / ~71%	~ 70	Centrifugation/ Filtration	[42]
Casein-GO	437.3	5 cycles / ~90%	~ 1600	Direct removal	[43]
GO–PLA	197.21	6 cycles/ ~75%	~ 60	Direct removal	This paper

3.7. Proposed Adsorption Mechanism. Based on the surface modification process and adsorption results, a possible mechanism for MB adsorption on the GO–PLA composite is proposed, as illustrated in Fig. 8. NaOH etching introduces abundant –OH and –COOH functionalities onto the PLA surface, which increases surface polarity and roughness, thereby enhancing interfacial adhesion. The subsequent grafting of KH550 introduces chemically active Si-O-C and Si-O-Si bonds, offering anchoring sites that enable robust immobilization of GO on the modified surface. GO is uniformly distributed and firmly attached to the modified PLA surface.

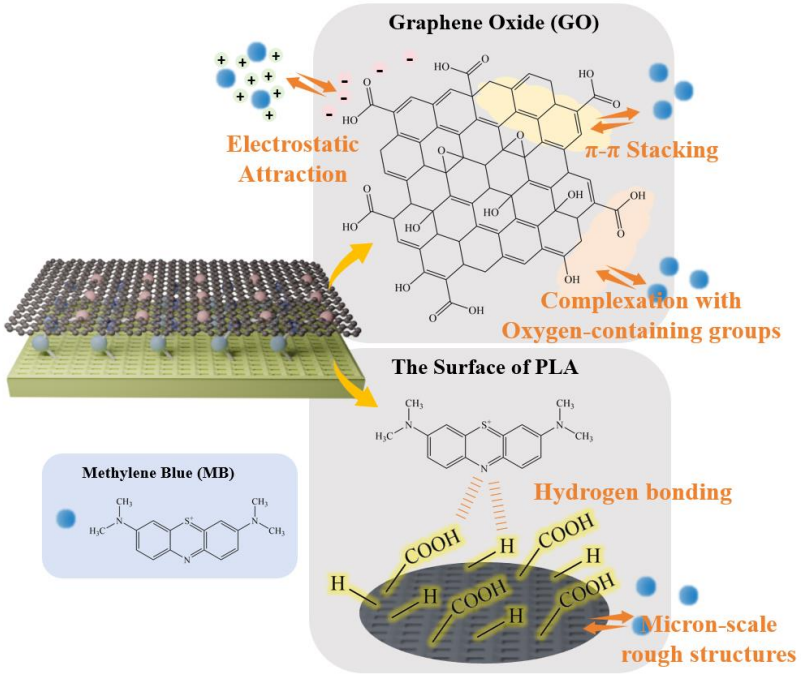


Fig. 8. Schematic diagram of adsorption mechanism.

During GO-based MB adsorption, multiple interactions are likely involved. Among them, π–π interactions between aromatic rings of MB and sp2-hybridized carbon domains of GO are considered one of the main adsorption pathways. In addition, oxygen-bearing functional groups on GO can serve as additional adsorption sites via weak hydrogen bonding or polar interactions with MB molecule. Electrostatic attraction further contributes under conditions where GO surface groups are deprotonated, promoting the electrostatic attraction between cationic MB molecules and the negatively charged surface [5, 36, 39, 43-45].

Consistent with these studies, the GO-PLA composite exhibits adsorption characteristics with Langmuir monolayer behavior and pseudo-second-order kinetics. The retention of oxygen-containing functional groups as revealed by the spectra is compatible with the co-action of these mechanisms. Finally, the micro-rough structures generated by NaOH etching enhance the accessible surface area and provide more available adsorption sites. Therefore, the adsorption behavior of the GO–PLA composite is possibly governed by the combined effects of π–π interaction, polar interaction, electrostatic attraction, and surface microstructural enhancement.

It should be acknowledged that the present mechanistic discussion is based on structural characterization and established literature precedents, rather than on direct spectroscopic or electrokinetic evidence of the adsorbate–adsorbent interface. Techniques such as X-ray photoelectron spectroscopy (XPS) before and after MB adsorption would provide direct evidence of chemical state changes at the GO surface; zeta potential measurements as a function of pH would quantify the electrostatic contribution; and pH-dependent adsorption studies would deconvolve the relative contributions of electrostatic versus non-electrostatic interactions. These investigations, together with density functional theory (DFT) calculations to quantify the energetics of individual interaction modes, are planned as part of our ongoing work.

4. Conclusion

A stable and environmentally friendly GO–PLA composite was successfully fabricated via an interfacial regulation strategy combining alkaline etching and silane coupling modification of the PLA substrate. The combined NaOH etching and KH550 modification significantly enhanced the surface free energy of PLA and promoted the uniform immobilization of GO, as confirmed by SEM, FTIR, Raman, and XRD analyses. This immobilization strategy surpasses several practical limitations associated with suspended GO in aqueous treatment systems.

The resulting composite showed good stability under both neutral and acidic conditions, rapid MB adsorption, and acceptable reusability. The adsorption behavior was well described by the pseudo-second-order kinetic model and the Langmuir isotherm model. The immobilized GO layer retained its functional activity after integration with the PLA substrate. This study provides a practical route for developing biodegradable and recyclable GO-based adsorbents through interfacial stabilization on polymer substrates, and it offers useful guidance for the design of other surface-immobilized GO-based materials.

Acknowledgments: The author gratefully acknowledges Guoping Li from the School of Materials Science and Engineering at Beijing Institute of Technology for providing laboratory facilities, experimental reagents, and instrument support for this work. The author also gratefully acknowledges his mentor, Jie Song from the expert supervision and mentorship throughout the project.

5. References

1. A. Tkaczyk, K. Mitrowska, and A. Posyniak, Synthetic organic dyes as contaminants of the aquatic environment and their implications for ecosystems: a review, *Sci Total Environ*, **717,** 137222 (2020). https://doi.org/10.1016/j.scitotenv.2020.137222
2. R. Rashid, I. Shafiq, P. Akhter, et al. A state-of-the-art review on wastewater treatment techniques: the effectiveness of adsorption method, *Environ Sci Pollut Res*, **28,** 9050–9066 (2021). https://doi.org/10.1007/s11356-021-12395-x
3. A. T. Smith, A. M. LaChance, S. Zeng, et al. Synthesis, properties, and applications of graphene oxide/reduced graphene oxide and their nanocomposites, *Nano Mater Sci*, **1**(1), 31–47 (2019). https://doi.org/10.1016/j.nanoms.2019.02.004
4. S. O. Abioye, Y. Majooni, M. Moayedi, et al. Graphene-based nanomaterials for the removal of emerging contaminants of concern from water and their potential adaptation for point-of-use applications, *Chemosphere*, **355,** 141728 (2024). https://doi.org/10.1016/j.chemosphere.2024.141728
5. C. Bulin, and T. Guo, Partially reduced graphene oxide as an efficient adsorbent towards ionic dyes and interaction mechanism, *J Mol Liq*, **391,** 123436 (2023). https://doi.org/10.1016/j.molliq.2023.123436
6. A. Nouri, W. L. Ang, E. Mahmoudi, et al. Decoration of polylactic acid on graphene oxide for efficient adsorption of methylene blue and tetracycline, *Chemosphere*, **322,** 138219 (2023). https://doi.org/10.1016/j.chemosphere.2023.138219

7. A. Paton-Carrero, P. Sanchez, L. Sánchez-Silva, and A. Romero, Graphene-based materials behaviour for dyes adsorption, *Mater Today Commun*, **30,** 103033 (2022). https://doi.org/10.1016/j.mtcomm.2021.103033
8. P. Vassileva, D. Vassileva, D. Kichukova, et al. A highly efficient graphene-based material for the removal of cationic dyes from aqueous solutions, *Materials*, **18,** 853 (2025). https://doi.org/10.3390/ma18040853
9. J. Ma, Q. Meng, A. Michelmore, et al. Covalently bonded interfaces for polymer/graphene composites, *J Mater Chem A*, **1,** 4255–4264 (2013). https://doi.org/10.1039/c3ta01277h
10. S. Qamar, N. Ramzan, and W. Aleem, Graphene dispersion, functionalization techniques and applications: a review, *Synth Met*, 307, 117697 (2024). https://doi.org/10.1016/j.synthmet.2024.117697
11. C. Y. Liu, H. Y. Liu, A. R. Xu, et al. In situ reduced and assembled three-dimensional graphene aerogel for efficient dye removal, *J Alloys Compd*, **714,** 522–529 (2017). https://doi.org/10.1016/j.jallcom.2017.04.245
12. S. Chang, Q. Zhang, Y. Lu, et al. High-efficiency and selective adsorption of organic pollutants by magnetic $CoFe_2O_4$/graphene oxide adsorbents: experimental and molecular dynamics simulation study, *Sep Purif Technol*, **238,** 116400 (2020). https://doi.org/10.1016/j.seppur.2019.116400
13. N. R. dos Santos, G. P. Gongora, J. S. de Sousa, et al. Application of three-dimensional structures of polylactic acid (PLA) impregnated with graphene oxide for adsorption of ibuprofen, *J Water Process Eng*, **78,** 108672 (2025). https://doi.org/10.1016/j.jwpe.2025.108672
14. B. Kim, D. Oh, T. Kim, et al. Fabrication of 3D-printed PLA filter with immobilized Prussian blue for aqueous cesium removal, *J Water Process Eng*, **55,** 104245 (2023). https://doi.org/10.1016/j.jwpe.2023.104179
15. T. D. Ngo, A. Kashani, G. Imbalzano, et al. Additive manufacturing (3D printing): a review of materials, methods, applications and challenges, *Compos Part B Eng*, **143,** 172–196 (2018). https://doi.org/10.1016/j.compositesb.2018.02.012
16. E. Feghali, L. Tauk, P. Ortiz, et al. Catalytic chemical recycling of biodegradable polyesters, *Polym Degrad Stab*, **179,** 109241 (2020). https://doi.org/10.1016/j.polymdegradstab.2020.109241
17. S. S. Park, Y. S. Lee, S. W. Lee, et al. Facile surface treatment of 3D-printed PLA filter for enhanced graphene oxide doping and effective removal of cationic dyes, *Polymers*, **15,** 269 (2023). https://doi.org/10.3390/polym15020269
18. A. Rahmatpour, and A. H. A. Hesarsorkh, Self-assembly of graphene oxide containing bio-nanocomposite hydrogels for removal of chlorpyrifos and methylene blue, *Int J Biol Macromol*, **320,** 145850 (2025). https://doi.org/10.1016/j.ijbiomac.2025.145850
19. P. P. Pereira, I. P. Gonçalves, L. V. A. Braz, et al. Removal of anionic dyes from lightly colored solutions with 3D printed ultrafiltration PLA membrane, *Water Air Soil Pollut*, **237,** 30 (2026). https://doi.org/10.1007/s11270-025-08731-3
20. M. Pastrafidou, V. Binas, I. A. Kartsonakis. Designing the Next Generation: A Physical Chemistry

Approach to Surface Coating Materials, *Appl Sci*, **15**, 10817 (2025). https://doi.org/10.3390/app151910817

21. M. M. Sabee, N. Kamalaldin, B. Yahaya, and Z. A. Hamid, Characterization and in vitro study of surface modified PLA microspheres treated with NaOH, *J Polym Mater*, **33,** 191–200 (2016).
22. J. Yang, Y. Wan, C. Tu, et al. Enhancing the cell affinity of macroporous poly(L-lactide) cell scaffold by a convenient surface modification method, *Polym Int*, **52,** 1892–1899 (2003). https://doi.org/10.1002/pi.1272
23. G. S. Bang, S. Cho, N. Kim, et al. Pyridinic-N-doped graphene paper from perforated graphene oxide for efficient oxygen reduction, *ACS Omega*, **3,** 5522–5530 (2018). https://doi.org/10.1021/acsomega.8b00400
24. X. Liu, L. Chen, Z. Liu, et al. Optimization of thermal and hydrophobic properties of GO-doped epoxy nanocomposite coatings, *Nanotechnol Rev*, **10,** 1236–1252 (2021). https://doi.org/10.1515/ntrev-2021-0078
25. A. Rudawska, and E. Jacniacka, Analysis for determining surface free energy uncertainty by the Owen–Wendt method, *Int J Adhes Adhes*, **29,** 451–457 (2009). https://doi.org/10.1016/j.ijadhadh.2008.09.008
26. C.Y. Tham, Z. A. A. Hamid, Z. Ahmad, and I. Hanafi, Surface modification of poly(lactic acid) (PLA) via alkaline hydrolysis degradation, *Adv Mater Res*, **970,** 324–327 (2014). https://doi.org/10.4028/www.scientific.net/AMR.970.324
27. J. Liu, and S. Jiang, Effect of sodium hydroxide and acetone pretreatments on the adhesion of three-dimensional printed polylactic acid filaments on linen and polyester fabrics, *Text Res J*, **93,** 161–171 (2022). https://doi.org/10.1177/00405175221116154
28. M. Schneider, N. Fritzsche, A. Puciul-Malinowska, et al. Surface etching of 3D printed poly (lactic acid) with NaOH: a systematic approach, *Polymers*, **12,** 1711 (2020). https://doi.org/10.3390/polym12081711
29. Z. Wu, P. P. Thoresen, L. Matsakas, et al. Facile synthesis of lignin-castor oil-based oleogels as green lubricating greases with excellent lubricating and antioxidation properties, *ACS Sustainable Chem Eng*, **11,** 12692–12702 (2023). https://doi.org/10.1021/acssuschemeng.3c01801
30. C. Liu, J. Song, G. Zhao, and Q. Ding, Improving surface wear resistance of polyimide by inserting KH550 grafted GO, *Polymers*, **15,** 2577 (2023). https://doi.org/10.3390/polym15112577
31. J. Li, S. Wang, S. Zhu, et al. Effect of KH-550 modified reduced graphene oxide (MrGO) content on the corrosion resistance behavior of MrGO/epoxy coatings in CO_2-Cl- environment, *Int J Electrochem Sci*, **17,** 22069 (2022). https://doi.org/10.20964/2022.06.07
32. T. Liu, Z. Li, X. Wang, and L. Zhang, MgO modified ordered porous materials for efficient methylene blue adsorption: effects of support, synthesis temperature and method on adsorption performance, *Colloids Surf A Physicochem Eng Asp*, **728,** 138514 (2026). https://doi.org/10.1016/j.colsurfa.2025.138514
33. H. O. Orugba, F. G. Sede, O. S. Oladeji, et al. In-situ and ex-situ synthesized activated carbons derived

from Raphia hookeri kernels for ibuprofen adsorption in wastewater, *Desalin Water Treat*, **319,** 100534 (2024).
https://doi.org/10.1016/j.dwt.2024.100534

34. H. Shi, W. Li, L. Zhong, and C. Xu, Methylene blue adsorption from aqueous solution by magnetic cellulose/graphene oxide composite: equilibrium, kinetics, and thermodynamics, *Ind Eng Chem Res*, **53,** 1108–1118 (2014). https://doi.org/10.1021/ie4027154
35. Y. Shi, G. Song, A. Li, et al. Graphene oxide–chitosan composite aerogel for adsorption of methyl orange and methylene blue: effect of pH in single and binary systems, *Colloids Surf A Physicochem Eng Asp*, **641,** 128595 (2022). https://doi.org/10.1016/j.colsurfa.2022.128595
36. H. M. Hassan, M. El-Aassar, M. A. El-Hashemy, et al. Sulfanilic acid-functionalized magnetic graphene oxide as a robust adsorbent for the efficient adsorption of methylene blue from aqueous solution, *J Mol Liq*, **361,** 119603 (2022). https://doi.org/10.1016/j.molliq.2022.119603
37. H. Bousemat, S. Ziane-Hezil, S. Benatmane, et al. Experimental and modeling studies for the simultaneous removal anionic dyes in single and binary systems using activated clay, *Sci Rep*, **15,** 45512 (2025).
https://doi.org/10.1038/s41598-025-30039-9
38. J. I. Abdelghani, F. I. Khalili, N. N. Al-Hashimi, et al. A selection guide for efficient graphene oxide-composite adsorbents, *Water Cycle*, **5,** 234–246 (2024). https://doi.org/10.1016/j.watcyc.2024.06.001
39. A. Arias, M. Guevara, T. Tene, et al. The adsorption of methylene blue on eco-friendly reduced graphene oxide, *Nanomaterials*, **10,** 681 (2020). https://doi.org/10.3390/nano10040681
40. W. Low, A. Nouri, S. F. Chua, et al. Immobilization of graphene oxide into microbead for fluidized-bed adsorption of methylene blue, *Desalination and Water Treatment*, **317,** 100135 (2024).
https://doi.org/10.1016/j.dwt.2024.100135
41. Dr. Allouss, Y. Essamlali, O. Amadine, et al. Response surface methodology for optimization of methylene blue adsorption onto carboxymethyl cellulose-based hydrogel beads: adsorption kinetics, isotherm, thermodynamics and reusability studies, *RSC Adv.*, **9,** 37858–37869 (2019).
https://doi.org/10.1039/c9ra06450h
42. F. E. Arias Arias, G. Tubon-Usca, M. Moreno-Samaniego, et al. Comparative adsorption of methylene blue on GO- and rGO-modified natural clinoptilolite: role of carbon oxidation state and pore blocking, *J. Mater. Sci.*, **61,** 7516–7544 (2026). https://doi.org/10.1007/s10853-026-12300-2
43. W. Xu, Y. Li, H. Wang, et al. Study on the adsorption performance of casein/graphene oxide aerogel for methylene blue, *ACS Omega*, **6,** 29243–29253 (2021). https://doi.org/10.1021/acsomega.1c04938
44. H. V. T. Luong, T. P. Le, T. L. T. Le, et al. A graphene oxide-based composite granule for methylene blue separation from aqueous solution: adsorption, kinetics and thermodynamic studies, *Heliyon*, **10,** e28648 (2024).
https://doi.org/10.1016/j.heliyon.2024.e28648
45. L. Ceroni, S. Pressi, L. Calvillo, et al. Ultrafast and reversible adsorption of methylene blue on covalently

sulfonated reduced graphene oxide, *Appl. Surf. Sci.*, **741,** 167074 (2026). https://doi.org/10.1016/j.apsusc.2026.167074